Федеральное государственное бюджетное образовательное учреждение
высшего образования
«Новосибирский государственный технический университет»
Кафедра полупроводниковых приборов и микроэлектроники

Паспорт
расчетно-графического задания (работы)

по дисциплине «Информационные технологии и основы программирования», 1 семестр

1. Методика оценки

Выполнение расчетно-графического задания (работы) (далее — РГЗ(Р)) является формой текущей аттестации (контроля) по дисциплине, предусмотренной учебным планом.

Цель РГЗ(Р): студентам необходимо отформатировать и подготовить к публикации текст научной статьи, выданной преподавателем. Статья предоставляется в pdf-формате на английском языке, переводить статью не требуется. Полученный текст следует перенести (вместе с рисунками, таблицами, формулами, элементами программного кода и т.д.) в программу Microsoft Word и отформатировать его в соответствии с предъявляемыми требованиями.

РГЗ(Р) выполняется индивидуально. Количество заданий достаточно для обеспечения, каждого обучающегося индивидуальным заданием РГЗ(Р).

Замена задания РГЗ(Р) осуществляется по согласованию с преподавателем из числа резервных (не занятых) заданий.

Преподаватель осуществляет руководство по выполнению задания, оказывает консультационную помощь и принимает отчет по РГЗ(Р), который состоит из следующих обязательных частей:

1) Титульный лист;
2) Основная часть в виде отформатированного текста.

Требования к оформлению общие для всех студентов и прилагаются к заданию в виде отдельного файла, приведенного в п. 5 настоящего Паспорта.

Отчет в электронном виде в установленные сроки сдается на кафедру для проверки. Преподаватель оценивает качество работы, отмечает положительные стороны и недостатки работы. При необходимости преподаватель возвращает РГЗ(Р) студенту для доработки и устанавливает сроки повторного предоставления для проверки, при этом студентом должны быть сделаны необходимые исправления и дополнения по всем замечаниям преподавателя.

По результатам проверки студенту выставляется оценка в соответствии с критериями, приведенными в п. 2 настоящего Паспорта. Оцениваемые позиции: соответствие отформатированного текста статьи предъявляемым требованиям по всем пунктам.

2. Критерии оценки результатов обучения, соотнесенных с уровнями освоения индикаторов достижения компетенций

Общие правила выставления оценок текущей аттестации определяются балльно-рейтинговой системой, установленной локальным актом НГТУ.

РГЗ(Р) считается выполненной **на продвинутом** уровне, если отформатирован весь объём предоставленного текста, и все требования к оформлению соблюдены с возможным наличием незначительных неточностей. Работа сдана преподавателю в указанные сроки и не возвращалась для доработки. Совокупность запланированных результатов и соотнесенных с ними индикаторов достижения компетенций не содержит пробелов. Закрепленные за РГЗ(Р) компетенции сформированы на продвинутом уровне. Оценка составляет **19–22** баллов.

РГЗ(Р) считается выполненной на **базовом** уровне, если отформатирован весь объём предоставленного текста, и большинство требований к оформлению соблюдены с возможным наличием незначительных ошибок. Работа сдана преподавателю в указанные сроки и однократно возвращалась студенту для незначительной доработки. Совокупность запланированных результатов и соотнесенных с ними индикаторов достижения компетенций содержит несущественные пробелы. Закрепленные за РГЗ(Р) компетенции сформированы на базовом уровне. Оценка составляет **16–18** баллов.

РГЗ(Р) считается выполненной на **пороговом** уровне, если отформатирован весь объём предоставленного текста и, как минимум, половина требований к оформлению соблюдены. Работа сдана преподавателю, но неоднократно возвращалась студенту для доработки. Совокупность запланированных результатов и соотнесенных с ними индикаторов достижения компетенций содержит существенные пробелы. Закрепленные за РГЗ(Р) компетенции сформированы на пороговом уровне. Оценка составляет **11–15** баллов.

РГЗ(Р) считается **невыполненной**, если отформатирован не весь объём предоставленного текста, большинство требований к оформлению не соблюдены или выполнены с существенными ошибками. Работа была сдана преподавателю, но неоднократно возвращалась студенту для доработки, что не привело к улучшению ее качества. Совокупность запланированных результатов и соотнесенных с ними индикаторов достижения компетенций содержит множественные существенные пробелы. Закрепленные за РГЗ(Р) компетенции не сформированы. Оценка составляет **менее 11** баллов.

3. Шкала оценки

В общей оценке по дисциплине баллы за РГЗ(Р) учитываются в соответствии с правилами балльно-рейтинговой системы, приведенными в рабочей программе дисциплины.

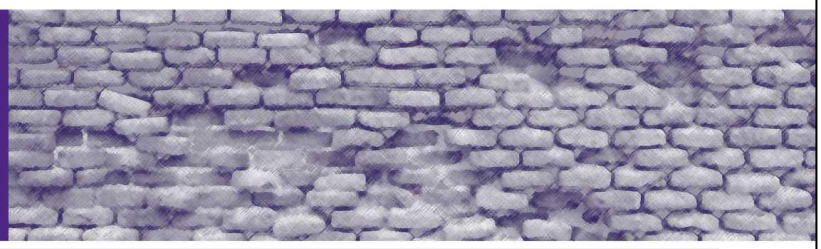
РГЗ(Р) как форма текущей аттестации (контроля) по дисциплине считается успешно выполненной, если сумма полученных баллов по всем его заданиям составляет от 11 до 22 баллов включительно.

4. Примерный вариант РГЗ(Р)

SYNOPSYS®

TCAD News

March 2009



Contents

3 Three-dimensional Single Event Effect Analysis of SRAM Cells

4 Making It Easier to Keep Up-to-Date with the Latest TCAD Sentaurus Application Notes on SolvNet®

Latest Edition

As this March issue goes to the presses, we look back on the first three months of this year as some of the most challenging many of us can remember. Along with most sectors of the economy, the semiconductor chip market has taken a severe hit and is now projected to decline this year. Yet, among all the gloomy clouds, silver linings are emerging. While it may be premature or unwise to speak of a near-term recovery, there are signs that, with inventories at very low levels, companies are beginning to grow orders. We can also feel confident that, in the midst of hardship, many of our customers have become even more efficient and focused. Cost control has been a pervasive theme. R&D has remained strong because companies realize that new products and innovation will bring differentiation as the recovery takes hold. At Synopsys, our commitment to help our customers develop new technologies and products in a cost-efficient and timely manner is stronger than ever.

The articles in this edition of *TCAD News* discuss two significant advances in the application of TCAD. The first article reviews the rapid progress achieved over the last few years in the simulation of multijunction solar cells. This type of solar cell holds the world efficiency record and is already being deployed in concentrator photovoltaic systems. The article illustrates how TCAD is used to design and optimize the complex device structure used in these cells. The second article highlights an issue that, while not well publicized, is of critical importance to satellite manufacturers and operators: the characterization and design of radiation-hardened electronics. As device dimensions shrink, novel ways to simulate radiation effects in semiconductors become necessary. In this article, recent advances in large-domain 3D simulations of SRAM cells are discussed.

We trust you will enjoy this issue of *TCAD News*, and we look forward to the next issue when Version C-2009.06 of TCAD Sentaurus will be featured.

With warm regards,



Terry Ma
VP Engineering, TCAD

Contact TCAD

For further information and inquiries: tcad_team@synopsys.com

Multijunction Solar-Cell Simulation Using TCAD Sentaurus

Introduction

Over the last few years, photovoltaic technology has experienced a resurgence due to the growing awareness of the impact of carbon emissions on the Earth's climate and the attendant need to develop clean energy sources. Among the many types of solar cell being researched and deployed in the field are multijunction designs. Initially developed for satellite solar panels, where high-efficiency and area are a premium and cost is a secondary consideration, multijunction solar cells hold the world record for efficiency.

On 14 January 2009, the Fraunhofer Institute for Solar Energy Systems (ISE) announced a new efficiency world record of 41.1% for a GaInP/GaInAs/Ge cell with a concentration factor of 454 suns [1], surpassing the previous record of 40.8% achieved by the National Renewable Energy Laboratory, a leading photovoltaic research laboratory in Colorado operated by the U.S. Department of Energy. Beyond the high efficiency, the work of Fraunhofer ISE also showed that buffer–substrate defects in metamorphic epitaxial layers do not appreciably degrade cell performance. By relaxing this constraint of having to match the substrate lattice constant, new combinations of ternary and quaternary compounds can be explored to improve performance further. As is well known, the common lattice-matched $Ga_{0.51}In_{0.49}P$/GaAs/Ge cell structure does not have an ideal bandgap configuration, and higher efficiencies should be possible by reducing the energy gap of the middle cell [2].

While triple-junction solar cells have been receiving considerable attention in connection with the reported world record efficiencies, dual-junction cells are under investigation as well. Recently, researchers at the Polytechnic University of Madrid reported a new world record of 32.6% efficiency for lattice-matched GaAs/GaInP cells at a high concentration of 1026 suns [3]. The researchers conducting this work believe that the lattice-matched design affords them the possibility of higher concentration, even exceeding 1000 suns, helping to lower the overall system cost. Moreover, optimization of the structure to achieve better current-matching between the top cell and bottom cell could boost the efficiency to approximately 35% [3].

In parallel with the aforementioned research, multijunction cells have been deployed in industrial concentrator photovoltaic (CPV) installations. Concentrator photovoltaics use a system of mirrors and lenses to focus the sunlight onto small, high-efficiency solar cells. The reduction of the active cell area effectively helps offset the higher production costs of multijunction cells.

One disadvantage of CPV systems resulting from the concentrating optics is the requirement for direct sunlight and clear skies for effective operation, making arid sunny climates optimal sites for deployment. Due to their cost-effectiveness, CPV systems are gaining greater relevance, as demonstrated by the latest installed systems in Spain [4] and in Israel, a first in the Middle East [5]. In the latter, using parabolic mirrors to achieve a concentration of approximately 800 suns, the system cleverly delivers electricity generated through photovoltaics and delivers hot water using the heat dissipated by the solar cells under illumination. Different versions of this system target a wide range of user profiles, from residential installations to large-scale electricity generation projects. This example is one among many CPV installations around the world, attesting to the brilliant possibilities for multijunction solar cells.

Why Simulate Multijunction Solar Cells?

These research and commercial successes beg the question: What is the role of numeric simulation in the development of multijunction solar cells? Several key factors point to a favorable answer.

First, there is the *development cost factor*. GaAs or Ge substrates are considerably more expensive than silicon, and the epitaxial growth rates are low in order to resolve accurately the sharp interfaces between materials. Moreover, epitaxial reactors, even multiwafer reactors, can grow only one type of structure at a time. Therefore, experimental splits are costly because of both substrate costs and one-sample-at-a-time epitaxial growth.

Second, there is the *design complexity factor*. Multijunction solar cells typically consist of 20 epitaxial layers or more, most of which play a critical role in the performance of the cell and must be designed precisely with respect to composition and thickness. Considering that for each layer a doping concentration, mole fraction, and thickness variable can be assigned, the total number of process variables to be optimized is large. In addition, some of the physical characteristics of these cells are very nonlinear, for example, the I–V characteristics of the tunnel diodes connecting the subcells, thereby rendering traditional optimization approaches reliant on polynomial fits to design-of-experiment splits impractical.

Instead, structural optimization approaches based on true physical models are required to capture the complex interplay of subcell thickness, tunnel-junction design, current-matching of the subcells, losses affecting external quantum efficiency (EQE), temperature-dependent effects, and so on. In addition, when it is considered that a 0.5% increase in efficiency is a worthwhile goal for next-generation multijunction solar cells, detailed physical modeling seems indeed justifiable.

Simulation Environment and Model Requirements

Not surprisingly, the simulation of multijunction solar cells combines aspects of generic solar cell and III–V compound device simulation. However, a few important requirements are noteworthy as they play a fundamental role in the usability and accuracy of the simulations.

Owing to the large number of epitaxial layers comprising the structure, an intuitive, easy-to-use environment for building the simulation structure is needed. In the TCAD Sentaurus environment, this is accomplished with the Epi utility, which works in conjunction with Sentaurus Structure Editor to easily create epitaxial multilayer stacks by specifying the layer properties in a comma-separated value (CSV) file. The utilization of ternary and quaternary compounds in multijunction cells motivates the need for user-defined material parameter files with arbitrary functional dependencies on mole fraction. The MatPar utility uses a tool command language (Tcl)–based framework for implementing user-defined models and material parameter files. Both these utilities are described in more detail in the next section.

From the perspective of physical models, thermionic emission across heterojunctions and transport in tunnel diodes are primary considerations. The design of tunnel diodes requires low electrical resistance, high optical transmissivity, and a high-enough peak-tunneling current density so as not to restrict current flow in the cell. They are built with highly doped (degenerate) p-n junctions with band-to-band tunneling and trap-assisted tunneling contributing to the current density.

Band-to-band tunneling can be implemented with local or nonlocal models. With local tunneling models, no actual carrier transport through the barrier occurs, and the tunneling is mimicked by adding an extra generation term to the continuity equation, typically dependent on the electric field or quasi–Fermi level gradient. These models have been applied successfully to MOS devices.

Nonlocal tunneling models, on the other hand, involve real spatial carrier transport through barriers and the use of a quantum-mechanical calculation of the tunneling probability along the tunneling path. A detailed investigation of band-to-band tunneling in the tunnel diodes used in multijunction solar cells indicates that nonlocal tunneling is necessary to match experimental I–V characteristics [6]. In particular, this work illustrates that while the local tunneling model showed a saturation of the derivative of the I–V curve at V = 0, in contradiction to experiment, the nonlocal tunneling model matched the measurement. By calibrating the effective Richardson constant and the conduction-band and valence-band tunneling masses, the authors obtained a good match of the measured I–V characteristics, particularly in the low forward-bias region where these diodes operate within the cell.

Recent Simulation Works

While Sentaurus Device already had a good reputation for simulating III–V single junctions [7], encouraging results in modeling a dual-junction solar cell have been achieved recently by carefully describing the band-to-band tunneling of the tunnel diode [8]. The simulation showed an excellent match to the measured I–V and EQE versus wavelength curves,

attesting to the physical comprehensiveness of the model. Key insights into the influence of the tunnel diode and top-cell thickness on EQE were discussed as well.

Yet another paper presented at the same conference tackled the important topic of temperature-dependent behavior of III–V solar cells [9]. In view of the high concentrations of sunlight under which these cells are designed to operate, a comprehensive understanding of the temperature-dependent behavior is very useful to optimize the structures. By incorporating a temperature-dependent absorption coefficient, energy gap, density-of-states, and carrier densities, the authors matched closely EQE versus wavelength curves at three temperatures (200 K, 300 K, and 400 K) and were able to point to the main physical sources of efficiency loss at higher temperatures [9].

These publications, key among others in the field, indicate that the simulation of III–V solar cells has made great progress in the last year and is ready to play an active role in the research and development of these important devices.

Structure Generation with Epi and MatPar

This part of the article presents a discussion of the practical aspects of multijunction solar-cell simulation in TCAD Sentaurus. As previously mentioned, the multilayer epitaxial structure can be created with the Tcl-based utilities Epi and MatPar [10]. Epi allows users to define the multilayer stack with a CSV file, and then it generates a Scheme script file that contains commands for Sentaurus Structure Editor to create a two-dimensional (2D) or three-dimensional (3D) multilayer stack.

Sentaurus Structure Editor creates a complete device from the multilayer stack by using normal operations such as etching contact windows through dielectric layers and adding electrical contacts. After the structure is created, the generated mesh and doping information is stored in a TDR file and is passed to Sentaurus Device. MatPar creates the main parameter file required by Sentaurus Device, consisting of user-defined parameter files grouped by material or region. The application note describing these utilities contains detailed information on usage [10]. In addition, Epi and MatPar form an integral part of a more recent application note on the simulation of a GaInP/GaAs/InGaAs triple-junction solar cell [11]. The structure used in this application note, which is analyzed in the next section, is shown in Figure 1.

Electrical and Optical Analysis

Optical and electrical calculations in Sentaurus Device can be performed in one step to compute relevant performance characteristics such as I–V, efficiency, and fill factor under specific illumination conditions. For the simulation of planar devices, the transfer matrix method can be used to calculate the optical field in devices consisting of multiple materials. The layers in the monolithic structure consist of various materials such as AlInP, GaInP, AlGaAs, GaAs, and InGaAs.

The light current–voltage (I–V) curve can be simulated for standard solar spectra (AM0, AM1.5g, and AM1.5d) and arbitrary concentrations. All the solar-cell structures can be simulated in one-dimensional (1D), 2D, or 3D simulation mode.

In 1D simulation mode, a homogeneous 2D structure is created with only two vertical mesh lines. Simulations performed in 1D simulation mode are relatively faster and can be used for the efficient bandgap engineering of the triple-junction solar cell. The 1D simulation mode can also be useful for a fast optimization of the simulation mesh in the y-direction.

The material parameters critical for solar cells, such as minority carrier mobility, minority carrier lifetime, and absorption coefficient, can be verified for the subcell materials – $Ga_{0.5}In_{0.5}P$, GaAs, and $In_{0.3}Ga_{0.7}As$ – using the Material Parameter Plotter as shown in Figure 2. The plots of these parameters are helpful in designing the triple-junction solar cell.

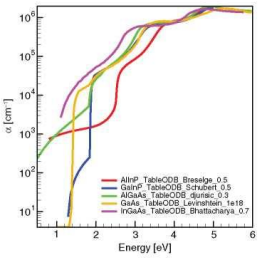


Figure 2. Absorption coefficient as a function of wavelength for $Al_{0.5}In_{0.5}P$, $Ga_{0.5}In_{0.5}P$, $Al_{0.3}Ga_{0.7}As$, GaAs, and $In_{0.3}Ga_{0.7}As$.

In addition to invoking the nonlocal tunneling model, the simulation of the tunnel diode requires a fine mesh around the tunnel junction to resolve mole and doping profiles accurately.

The I–V curve of the tunnel diode is shown in Figure 3. The negative differential resistance region is clearly seen. At zero bias, the current is zero. As the forward-bias voltage increases, the current increases and reaches a peak value. With a further increase in the bias voltage, the current decreases to zero in the negative differential resistance region. As required, the peak-tunneling current density is much larger than that of the triple-junction solar cell.

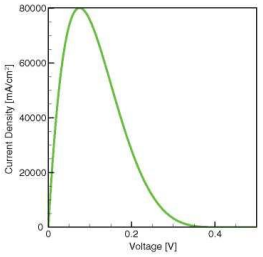


Figure 3. I–V characteristics of AlGaAs/GaAs tunnel diode.

The I–V curves of all the stacked subcells under AM1.5d illumination are shown in Figure 4. This plot is useful to verify the current-matching of the cells. The light I–V and P–V curves of the complete triple-junction solar cell under AM1.5d illumination are shown in Figure 5.

The reflectance of the triple-junction solar cell and EQE of the stacked subcells are shown in Figure 6. The EQE of each subcell dominates in a particular wavelength region up to the characteristic wavelength of its band gap: the top GaInP subcell up to 0.68 µm, the middle GaAs subcell up to 0.87 µm, and the bottom InGaAs subcell up to 1.2 µm. The steep cross-overs in the EQE between the subcells exist due to the high absorption that the direct bandgap materials offer. Only the cross-over between the top and middle subcells in the wavelength range from 0.45 to 0.65 µm shows smooth behavior. This demonstrates the effect of current-matching due to top-cell thinning. By using a thinned top cell, a part of the blue light, usually attributed to the top cell, can surpass the top cell and contribute to the current in the middle cell to achieve current-matching. The wavy-shaped EQE of the bottom cell in Figure 6 is due to optical interference effects.

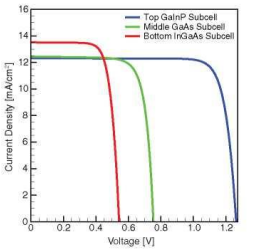


Figure 4. Light I–V characteristics of stacked subcells under AM1.5d illumination.

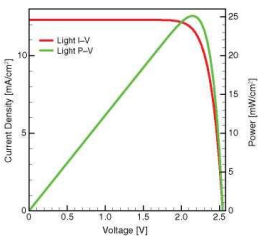


Figure 5. Light I–V and P–V characteristics of triple-junction solar cell under AM1.5d illumination.

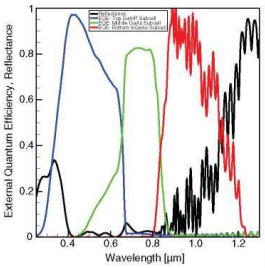


Figure 6. EQE spectra of subcells and reflectance spectrum of GaInP/GaAs/InGaAs triple-junction solar cell.

Conclusion

Multijunction solar cells hold the world record for efficiency and continue to be developed for deployment in CPV systems. Recent model development and simulation case studies of multijunction solar cells demonstrate the value of TCAD Sentaurus in the design and optimization of these important photovoltaic devices.

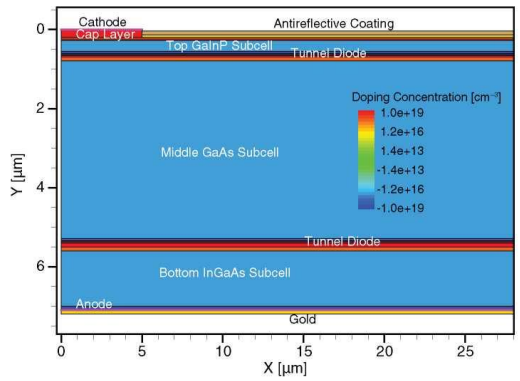


Figure 1. Smallest symmetry element of triple-junction solar cell generated by Sentaurus Structure Editor.

References

[1] "Fraunhofer breaks world conversion record," *PV Magazine*, no. 2, p. 48, February 2009.

[2] F. Dimroth, U. Schubert, and A. W. Bett, "25.5% Efficient $Ga_{0.35}In_{0.65}P/Ga_{0.83}In_{0.17}As$ Tandem Solar Cells Grown on GaAs Substrates," *IEEE Electron Device Letters*, vol. 21, no. 5, pp. 209–211, 2000.

[3] "Madrid team sets dual-junction solar record," *Compound Semiconductor*, article available online at <http://compoundsemiconductor.net/cws/article/news/36640>, published November 2008.

[4] "Concentrix Solar und Abengoa Solar bringen erfolgreich gemeinsames 2-MW-Kraftwerk in Spanien ans Netz," article available online at <http://www.concentrix-solar.de/news/newssingle/seite/1/artikel/concentrix-solar-und-abengoa-solar-bringen-erfolgreich-gemeinsames-2-mw-kraftwerk-in-spanien-ans-net>, March 2009.

[5] "High-concentration at home," *PV Magazine*, no. 2, pp. 50–52, February 2009.

[6] M. Hermle *et al.*, "Numerical Simulation of Tunnel Diodes and Multi-Junction Solar Cells," in *33rd IEEE Photovoltaic Specialists Conference*, San Diego, CA, USA, May 2008.

[7] G. Létay, M. Hermle, and A. W. Bett, "Simulating Single-junction GaAs Solar Cells Including Photon Recycling," *Progress in Photovoltaics: Research and Applications*, vol. 14, no. 8, pp. 683–696, 2006.

[8] S. P. Philipps *et al.*, "Numerical Simulation and Modeling of III-V Multi-Junction Solar Cells," in *23rd European Photovoltaic Solar Energy Conference and Exhibition*, Valencia, Spain, September 2008.

[9] S. P. Philipps *et al.*, "Characterization and Numerical Modeling of the Temperature-dependent Behavior of GaAs Solar Cells," in *23rd European Photovoltaic Solar Energy Conference and Exhibition*, Valencia, Spain, September 2008.

[10] *Template for Creating and Simulating Mutilayered Heterostructure Devices with TCAD Sentaurus*, TCAD Sentaurus application note, available from SolvNet® at <https://solvnet.synopsys.com/retrieve/023480.html>, March 2009.

[11] *Simulation of Triple-Junction GaInP/GaAs/InGaAs Solar Cells with Transfer Matrix Method*, TCAD Sentaurus application note, available from SolvNet at <https://solvnet.synopsys.com/retrieve/025891.html>, March 2009.

■

Three-dimensional Single Event Effect Analysis of SRAM Cells

Introduction

Outer space is an inhospitable environment for semiconductor electronics. Charged particles trapped in the radiation belts and cosmic particles from outside the solar system with energies reaching several GeV can penetrate metal shielding in satellites and collide with the semiconductor chips inside the electronic systems. The result is a host of undesirable effects: spurious signals, corrupted data, latch-up, and device burnout. Clearly, providing adequate protection against radiation effects for semiconductor electronics in multimillion-dollar satellites is a mission-critical design problem, motivating design and processing techniques to address it. Yet, a semiconductor chip may be subjected to harmful radiation even on Earth. The surface of the Earth is exposed to high-energy cosmic rays and their decay products, and the neutron background flux is high enough to generate heavy-ion tracks inside the chip through nuclear spallation reactions when the neutrons collide with the host silicon atoms.

The characterization and modeling of radiation effects in semiconductors has become a highly technical field, employing specialized techniques at the circuit and device level. Advances in computer hardware and in the sophistication of TCAD tools have been adopted readily by the radiation effects community to lend more insight into the interaction of radiation with device behavior and to help device engineers optimize their device structures to improve the radiation hardening of semiconductor chips [1].

Numeric Simulation of Radiation Effects

Although early TCAD studies of radiation effects were performed in two dimensions, today three-dimensional (3D) analysis is more common in view of the tremendous progress in multicore hardware and parallel simulation algorithms, which have made 3D simulation practical.

The motivation for 3D simulation of radiation effects stems from the intrinsically 3D nature of the charge tracks and the coupling between multiple transistors in response to the particle strike. SRAM cells are particularly susceptible to the effects of particle strikes because of the potential for bit upset, commonly known as an SRAM single event upset (SEU). TCAD simulation of radiation effects in SRAM cells is complicated by the need to account for the behavior of all transistors in the cell.

Mixed-mode simulation, whereby the transistor receiving the strike is treated numerically and the remaining transistors are described with compact models, is a popular approach. Although, full 3D simulations of the entire SRAM domain have steadily gained acceptance [2]. Three-dimensional studies of radiation effects in SRAM cells include arbitrarily angled particle strikes, tracks due to secondary ions from neutron-induced spallation reactions [3], computation of SEU cross sections through sampling simulations across the entire SRAM cell domain [4], and evaluation of the impact of well design and well-tap layout frequency on multiple cell upsets [5].

SRAM SEU Analysis with TCAD Sentaurus

The application of TCAD Sentaurus to the analysis of a heavy-ion strike in an SRAM memory cell is now described using, as a basis, an application note available from SolvNet® [6].

The project is organized in Sentaurus Workbench and starts with the creation of a 3D SRAM cell using Sentaurus Structure Editor in process emulation mode, with the use of process flow–oriented structure generation commands, followed by meshing using Sentaurus Mesh, and electrical simulation with Sentaurus Device. Figure 1 shows the circuit schematic of the six-transistor CMOS SRAM cell. N1, N2, P1, and P2 form the cross-coupled inverter pair; while M5 and M6 form the access transistors.

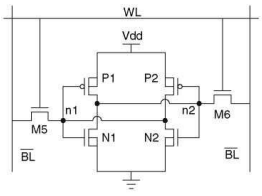


Figure 1. Circuit schematic of six-transistor CMOS SRAM cell.

Structure Generation

The 3D SRAM device structure is generated by a sequence of process emulation commands executed in Sentaurus Structure Editor. The Synopsys layout editor IC WorkBench EV Plus (ICWBEV Plus) is used to create or edit GDSII layout files that are subsequently used as input to the TCAD simulation. Using the layout file shown in Figure 2, a Sentaurus markup layer 'SRAM3D' is added in ICWBEV Plus to define a 3D simulation domain. Auxiliary layers are defined in ICWBEV Plus to denote the locations of the source, drain, and gate contacts for each of the transistors. This interactive use of Sentaurus Structure Editor and ICWBEV Plus is a convenient way to generate 3D structures based on a given layout.

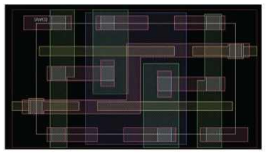


Figure 2. Layout of SRAM cell and 3D simulation domain.

This process is illustrated. First, the mask defining the active region is applied to etch the silicon trenches (see Figure 3a). Second, after filling the trenches with oxide, the PMOS threshold adjust implant is performed using the NWELL mask and the analytic implant capabilities of the process emulation mode of Sentaurus Structure Editor. The NWELL mask with opposite polarity is used for the threshold adjust implant in the NMOS devices. Subsequently, the polysilicon mask is used to pattern the gate oxide and to deposit polysilicon on the gate region (see Figure 3b). This is followed by an implant in the source and drain regions. Finally, the contact mask is used to define contacts (see Figure 3c).

ICWBEV Plus also allows the definition of auxiliary layers for layout-driven meshing. This capability is used in this project to refine the mesh at the gate oxide–silicon interface. Mesh generation is performed with the Sentaurus Mesh engine, which is part of Sentaurus Device. In view of the large simulation domain, a mesh strategy focusing on the critical device regions is used:

- Coarse mesh inside the substrate.
- Refinement on doping.
- Refinement at the silicon–gate oxide interface for the N1, N2, P1, and P2 transistors.

This strategy helps to reduce the node count, while not compromising accuracy. Figure 4 shows the discretized mesh structure.

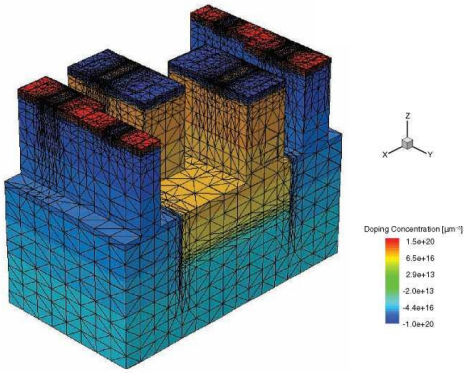


Figure 4. Device structure with mesh generated by Sentaurus Mesh: structure contains 44000 nodes and oxide region is not shown here for clarity.

Device Simulations of the SRAM Cell

Device simulations of the SRAM cell are performed in two steps. The first step demonstrates the working of the SRAM cell by writing data into the cell and biasing the cell in the off-state. In the second step, a logic '0' is written into the cell and the access transistors are switched off. Then, heavy ions bombard the drain of the off-state transistor N1, representing one of the most sensitive strike conditions. The characteristics of the strike – impact location, energy, angle, linear energy transfer, and radius – can be parameterized.

Sentaurus Device is used to simulate the time evolution of the voltage at different circuit nodes. A system description is required for circuit simulation. Electron–hole pair generation due to heavy-ion impact is nonlocal in nature; therefore, the SRAM cell is defined as one single system instead of six systems representing six transistors, realizing a true 3D mixed-mode simulation. Since this is a mixed-mode simulation, circuit and contact equations are solved, along with the Poisson equation and the electron and hole continuity equations, in a self-consistent manner.

The applied and output waveforms used to simulate the initial writing operation are shown in Figure 5. Voltage sources are connected to the power supply, bit line (BL), and word line (WL). Voltage sources connected to the WL and BL are ramped up slowly with a rise time of 1 µs to the final required voltage of 1.5 V. The bitbar line is connected to ground through a resistor of 10^8 Ω. This large resistance limits the current flowing through the bitbar line, effectively setting it to a near floating-node condition.

The second simulation studies the effect of a heavy-ion strike. First, the cell is written with a logic '0' and then the access transistors are switched off, putting the cell in a data-hold state. The heavy-ion model is then activated on the drain of transistor N1. To write '0' into the cell, the BL is grounded.

Figure 6 shows the applied waveforms for the power supply and WL, and the output

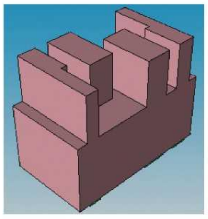


Figure 3a. Trench formation after silicon etching.

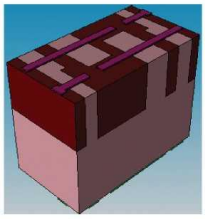


Figure 3b. Formation of shallow trench isolation and generation of polysilicon gate.

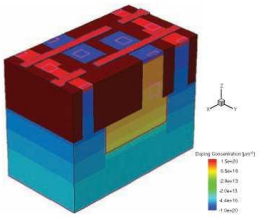


Figure 3c. Doping profile of final generated structure.

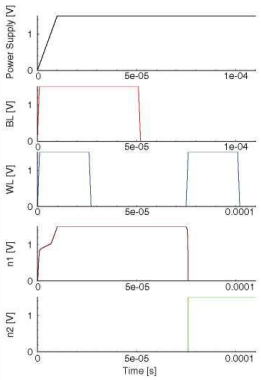


Figure 5. Voltage waveforms for power supply, BL, WL, and nodes n1 and n2 during initial writing operation.

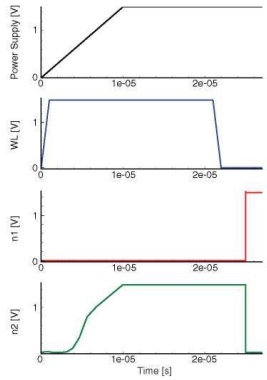


Figure 6. Voltage waveforms for power supply, WL, and nodes n1 and n2 during second stage.

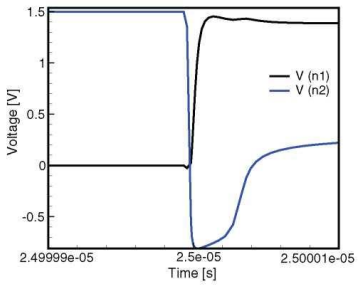


Figure 7. Node voltages versus time for NMOS drains as a result of a single event strike; the SRAM cell switches states.

waveforms at nodes n1 and n2. The heavy ion strikes the drain of transistor N1 at 2.5 x 10^{8} s. Figure 7 shows the flipping of the n1 and n2 node values following the heavy-ion strike. The physical mechanism leading to the node flipping, or bit upset, relies on the activation of a parasitic thyristor that effectively short-circuits the drain of N1 with the source of N1. As a result, the voltage of node n1 switches from 0 V to 1.5 V. This causes transistor N2 to switch off, and node n2 switches from 1.5 V to 0 V.

It is interesting to note that for this specific example, if a heavy ion bombards the drain of N2, a small deviation from the stable voltage values would be observed at the two nodes for a short time, and no flipping of nodes would be observed. This can be understood by realizing that, as soon as charges are created, they are swept to the ground since the channel N2 is in an on-state, preventing the parasitic thyristor from switching on.

Conclusion

Ionizing radiation poses significant reliability challenges to semiconductor chip operation, particularly in outer space. For many years, TCAD simulation has provided physical insight into radiation effects in semiconductor devices. Recent advances in computer hardware and 3D TCAD algorithms have enabled the simulation of multitransistor SRAM cells using a single physical structure.

References

[1] "An Efficient Simulation Environment for Modeling Single Event Effects with the Sentaurus Tool Suite," *TCAD News*, pp. 5–6, June 2007.

[2] Ph. Roche *et al.*, "SEU Response of an Entire SRAM Cell Simulated as one Contiguous Three Dimensional Device Domain," *IEEE Transactions on Nuclear Science*, vol. 45, no. 6, pp. 2534–2543, 1998.

[3] J.-M. Palau *et al.*, "Device Simulation Study of the SEU Sensitivity of SRAMs to Internal Ion Tracks Generated by Nuclear Reactions," *IEEE Transactions on Nuclear Science*, vol. 48, no. 2, pp. 225–231, 2001.

[4] P. E. Dodd *et al.*, "SEU-Sensitive Volumes in Bulk and SOI SRAMs From First-Principles Calculations and Experiments," *IEEE Transactions on Nuclear Science*, vol. 48, no. 6, pp. 1893–1903, 2001.

[5] G. Gasiot, D. Giot, and P. Roche, "Multiple Cell Upsets as the Key Contribution to the Total SER of 65 nm CMOS SRAMs and Its Dependence on Well Engineering," *IEEE Transactions on Nuclear Science*, vol. 54, no. 6, pp. 2468–2473, 2007.

[6] *Transient Simulation of Single Event Upset due to Heavy Ion Impact on 6T 3D SRAM Cell*, TCAD Sentaurus application note, available from SolvNet at <https://solvnet.synopsys.com/retrieve/024777.html>, March 2009.

■

Making It Easier to Keep Up-to-Date with the Latest TCAD Sentaurus Application Notes on SolvNet®

How many customers really know what Synopsys has to offer in terms of application notes that focus on different aspects of TCAD simulation?

Did you know that there are currently tens of TCAD Sentaurus application notes available from SolvNet and that more are added every month?

These application notes, covering many topics and tool flows, constitute a veritable library of best practices and techniques to help customers maximize their utilization of TCAD tools.

If you have never visited the site, registering for access to SolvNet is easy, and the benefits are substantial.

Why not take some time to do this today. Go to https://solvnet.synopsys.com, and follow the link on the home page.

To make it even easier to keep abreast of the latest additions to the collection, an index has been created that is updated regularly. The link is https://solvnet.synopsys.com/retrieve/026036.html.

Application notes are a great way to learn how TCAD Sentaurus can be applied to specific simulation tasks.

To browse and download application notes:

1. Go to https://solvnet.synopsys.com.
2. Click the **Browse Content** tab.
3. From the list of products, click **TCAD Sentaurus**.
4. Click **Application Note**.
5. Select how you want to sort the entries.

Application notes are accompanied by simulation projects that can be downloaded and executed by licensed users.

■

SYNOPSYS®

700 East Middlefield Road, Mountain View, CA 94043, USA
www.synopsys.com

Synopsys, the Synopsys logo, and SolvNet are registered trademarks of Synopsys, Inc. All other products or service names mentioned herein are trademarks of their respective holders and should be treated as such.
© 2009 Synopsys, Inc. All rights reserved. 03/2009.DGS.1000

Образец Оформления Статьи

I. ОФОРМЛЕНИЕ ТЕКСТА

ПЕРВАЯ БУКВА текста статьи оформляется с абзацного отступа 0,5 см как буквица (вкладка <Вставка> –> <Буквица> –> <В тексте>) с размером две строки. Первые два-три слова текста, начиная со второй буквы первого слова, пишутся заглавными буквами.

Параметры страницы следующие: размер бумаги — стандартный A4 (210 × 297 мм), верхнее и нижнее поля — 3 см, левое и правое поля — 2,5 см.

Основной текст набирается шрифтом Times New Roman 10 пунктов с одинарным междустрочным интервалом в две колонки шириной 7,75 см, расстояние между колонками — 0,5 см. Отступ первой строки — 0,5 см, выравнивание — по ширине, включая автоматическую расстановку переносов (вкладка <Макет> –> <Расстановка переносов> –> <Авто>).

Статья должна начинаться с заголовка, расположенного в центре (без абзацного отступа) и набранного шрифтом Times New Roman 24 пункта малыми прописными буквами с одинарным междустрочным интервалом, в жирном начертании, каждое слово с заглавной буквы. Переносы в заголовках не допускаются, точка в конце не ставится. После заголовка следует интервал 24 пункта. Отдельную пустую строку после заголовка оставлять не нужно. Новая статья начинается с новой страницы.

Разделы статьи нумеруются римскими цифрами по порядку, названия разделов располагаются в центре колонки (без абзацного отступа) и пишутся заглавными буквами шрифтом Times New Roman 10 пунктов с одинарным междустрочным интервалом. Переносы в названиях разделов не допускаются. В конце названия раздела точка не ставится. Интервал перед строкой названия раздела составляет 12 пунктов, после — 6 пунктов.

Страницы текста нумеруются в правом нижнем углу арабскими цифрами (вкладка <Вставка> –> <Номер страницы >) в формате: - 1 - (с дефисами) шрифтом Times New Roman 12 пунктов.

II. ОФОРМЛЕНИЕ ОБЪЕКТОВ

Оформление рисунков. Все рисунки должны быть перенесены в основной текст с помощью стандартных средств *pdf-Reader* (выделение рисунка) или путём снятия скриншота (клавиша *Print Screen*) с экрана монитора и последующей обрезки изображения в соответствующей программе.

Рисунки и фотографии должны быть чёткие, хорошего качества. Вставка рисунка осуществляется непосредственно в текст в режиме положения и обтекания <В тексте>, расположение рисунка поверх текста не допускается. При изготовлении рисунков средствами рисования текстового процессора их необходимо сгруппировать.

Ширина рисунка — 7,7 см, высота — пропорционально ширине, интервал до — 6 пт, интервал после — 6 пт.

В случае, когда рисунок имеет размеры, большие, чем ширина колонки, его следует, по возможности, сжать. Если же при этом теряются мелкие детали, рисунок можно расположить по центру страницы в одну колонку. Для этого необходимо прервать разбиение на колонки с помощью разрыва раздела (на текущей странице), вставить большой рисунок, а затем опять вернуться к разбиению текста на две колонки.

Расположение подрисуночных подписей внутри рисунка не допускается, подписи набираются непосредственно в тексте статьи с использованием шрифта Times New Roman 8 пунктов с одинарным междустрочным интервалом. Подписи к рисункам должны быть отформатированы по ширине с отступом первой строки 0,5 см. После подписи к рисунку следует отступ 6 пунктов.

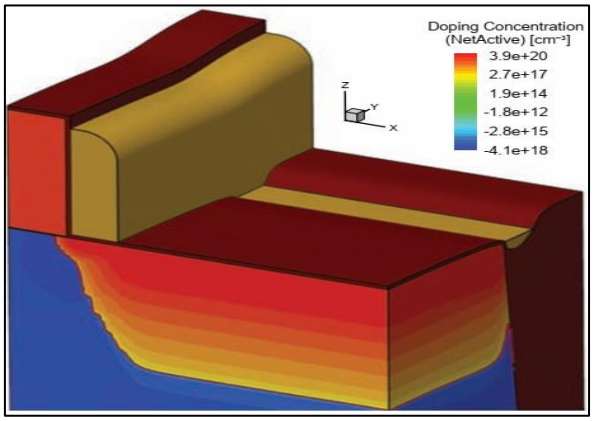


Figure 1: Phosphorus distribution in stand-alone P-FinFET (upper left corner) and 6T-FinFET SRAM cell after halo implantation.

Оформление таблиц. Таблицы должны быть перерисованы в текстовом процессоре как таблицы (они не вставляются как рисунки). Таблицы нумеруются римскими цифрами по порядку следования в тексте.

Слово «Таблица» и соответствующий ей номер таблицы пишутся заглавными буквами, шрифт Times New Roman 10 пунктов с одинарным междустрочным интервалом, и располагаются в центре колонки (без абзацного отступа). Интервал до слова «Таблица» — 6 пунктов, после слова «Таблица» — 0 пунктов.

Ниже, в центре следующей строки (также без абзацного отступа), располагается название таблицы в соответствии с её содержанием. Для написания названия таблицы используется шрифт Times New Roman 8 пунктов с одинарным междустрочным интервалом, название также пишется заглавными буквами, интервал до названия — 0 пунктов, после — 0 пунктов. Переносы в названии таблицы не допускаются, точка в конце не ставится.

TABLE I
THE TITLE OF TABLE IS WRITTEN HERE

	Column 1	Column 2	Column 3
Row 1	RC11	RC12	RC13
Row 2	RC21	RC22	RC23
Row 3	RC31	RC32	RC33

Шрифт для содержимого таблицы устанавливается Times New Roman 8 пунктов с одинарным междустрочным интервалом, интервал до — 0 пунктов, после — 0 пунктов. Таблица располагается по центру колонки. Максимальный размер таблицы по ширине равен 7,7 см.

Головка таблицы должна быть отделена двойной линией от остальной части таблицы. Высота строк таблицы должна быть не менее 5 мм. Обязательно необходимо вертикальное выравнивание текста внутри ячеек по центру: вкладка <Макет> для работы с таблицами –> <Выровнять по Центру>. Первый абзац после таблицы имеет интервал перед — 6 пунктов.

Широкие таблицы, так же, как и большие рисунки, занимающие две колонки, следует вставлять по центру всего листа, прерывая разбиение текста на колонки.

Оформление формул. Формулы набираются в специальном редакторе формул MathType (он требует отдельной установки в Windows). Интервал до формулы — 6 пт, интервал после — 6 пт. При этом следует придерживаться настроек программы, указанных на рис. 2 и рис. 3 сверху справа.

Формулы должны форматироваться по правому краю колонки и располагаться в её центре с помощью табуляции, например:

$$A(s) = \sum_{i=0}^{n^2+3} A_i s^{(i+1)^2} + \alpha \ . \qquad (1)$$

Если выровнять абзац с формулой и её номером по правому краю, то поставив между ними знак табуляции и кликнув курсором на линейке вверху, на ней появится «уголок табуляции». Перемещая уголок табуляции по линейке, можно регулировать расстояние между формулой и её номером. Используется сквозная нумерация формул по порядку следования. Если ссылки на формулу не предусмотрены по тексту, формула не нумеруется.

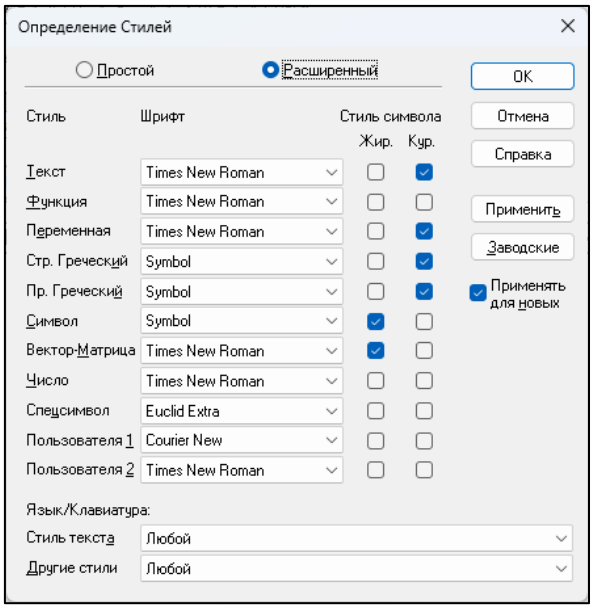


Рисунок 2: Установки меню «Стиль» специального редактора формул MathType.

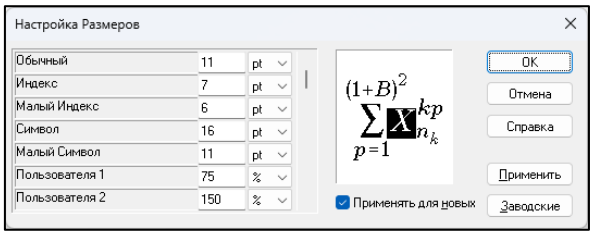


Рисунок 3: Установки меню «Размер» специального редактора формул MathType.

В случае, если длина формулы превышает ширину колонки, то применяется её перенос на следующую строку. Если её длина по-прежнему превышает ширину колонки, в этом случае автору следует вводить дополнительные промежуточные переменные и функции, не пересекающиеся по обозначению с уже используемыми по тексту. Знаки препинания, необходимые для связи формулы с текстом, пишутся вне самой формулы.

III. ПРОЧЕЕ

Элементы программного кода, если таковые имеются, должны быть отделены от основного текста интервалами 6 пт (только первая и последняя строки). Используемый для оформления шрифт — `Courier New`, 10 пт, например:

```
#include <iostream>
using namespace std;
int main () {
    cout << "Hello, World!";
    cout << endl << endl;
    system("pause");
    return 0;
}
```

В числовых интервалах физических величин вместо дефиса ставится знак многоточие, например, 40…50 см. Символ «÷» никогда не используется. Вместо него используется короткое тире (Ctrl + Минус на доп. клавиатуре) без пробелов. Кроме того, оно обозначает интервал «от – до», например, январь – февраль 1992 г., в течение 3–5 с, в работах [1–3].

Математические знаки действий и соотношений, за исключением наклонной черты дроби, отделяются пробелами от смежных символов или чисел, кроме случаев, когда такие знаки обозначают положительное или отрицательное значение, степень увеличения и др., например, точность определения температуры кипения ±1,5 °С, в течение ~20 мин., этанол : вода = 1 : 1, кратность ×200.

Сокращения из нескольких слов разделяются пробелами, за исключением самых общеупотребительных (и т.д., и т.п., т.е.).

Аббревиатуры, употребляемые как прилагательные, пишутся через дефис, например, ИК-спектроскопия, ПЭ-плёнка, ЖК-состояние. Аббревиатуры пишутся единообразно по всей статье, например, ЭДС или э.д.с., КПД или к.п.д.

В качестве разделителя целой и дробной части числа всегда используется запятая: 5,25. Градусы Цельсия: 5 °С, а не 5°. Угловые градусы никогда не опускаются: 5° – 10°, а не 5–10°; на осях рисунков: θ, град, а не θ°. Размерности переменных пишутся через запятую (E, кДж/моль).

IV. ОБСУЖДЕНИЕ РЕЗУЛЬТАТОВ

Необходимо, чтобы на последней странице статьи высота колонок была одинаковой.

Список литературы указывается отдельным ненумерованным разделом. Шрифт списка литературы — Times New Roman 8 пунктов.

REFERENCES

[1] Бакут П.А., Жулина Ю.В., Иванчук Н.А. Обнаружение движущихся объектов/ Под ред. П.А. Бакута. — М.: Сов. радио, 1980. — 288 с.

[2] Pattern Classification Pattern Classification, Duda Richard O., Hart Peter, Stork David G. — 2nd ed. — USA: John Wiley & Sons, 2001, p. 738.

[3] Реутов С., Сафронов Е. Комплектные поставки орудий труда как средство создания системы машин // Вопр. экономики, 1985. № 1. С 57-67.

[4] Stewartson K. On the flow near the trailing edge of a flat plate // Proc. Roy. Sec. London. Ser. A. 1968. V. 306. No. 1486. P. 275-290.